JOURNAL OF THE AMERICAN COLLEGE OF CARDIOLOGY VOL. 73, NO. 12, 2019

PUBLISHED BY ELSEVIER

THE PRESENT AND FUTURE

JACC STATE-OF-THE-ART REVIEW

Anatomy, Function, and Dysfunction of the Right Ventricle

JACC State-of-the-Art Review

Javier Sanz, MD,[a,b] Damián Sánchez-Quintana, MD, PhD,[c] Eduardo Bossone, MD, PhD,[d] Harm J. Bogaard, MD, PhD,[e] Robert Naeije, MD, PhD[f]

JACC JOURNAL CME/MOC/ECME

This article has been selected as the month's *JACC* CME/MOC/ECME activity, available online at http://www.acc.org/jacc-journals-cme by selecting the *JACC* Journals CME/MOC/ECME tab.

Accreditation and Designation Statement

The American College of Cardiology Foundation (ACCF) is accredited by the Accreditation Council for Continuing Medical Education to provide continuing medical education for physicians.

The ACCF designates this Journal-based CME activity for a maximum of 1 *AMA PRA Category 1 Credit(s)*™. Physicians should claim only the credit commensurate with the extent of their participation in the activity.

Successful completion of this CME activity, which includes participation in the evaluation component, enables the participant to earn up to 1 Medical Knowledge MOC point in the American Board of Internal Medicine's (ABIM) Maintenance of Certification (MOC) program. Participants will earn MOC points equivalent to the amount of CME credits claimed for the activity. It is the CME activity provider's responsibility to submit participant completion information to ACCME for the purpose of granting ABIM MOC credit.

Anatomy, Function, and Dysfunction of the Right Ventricle: *JACC* State-of-the-Art Review will be accredited by the European Board for Accreditation in Cardiology (EBAC) for 1 hour of External CME credits. Each participant should claim only those hours of credit that have actually been spent in the educational activity. The Accreditation Council for Continuing Medical Education (ACCME) and the European Board for Accreditation in Cardiology (EBAC) have recognized each other's accreditation systems as substantially equivalent. Apply for credit through the post-course evaluation. While offering the credits noted above, this program is not intended to provide extensive training or certification in the field.

Method of Participation and Receipt of CME/MOC/ECME Certificate

To obtain credit for *JACC* CME/MOC/ECME, you must:

1. Be an ACC member or *JACC* subscriber.
2. Carefully read the CME/MOC/ECME-designated article available online and in this issue of the *Journal*.
3. Answer the post-test questions. A passing score of at least 70% must be achieved to obtain credit.
4. Complete a brief evaluation.
5. Claim your CME/MOC/ECME credit and receive your certificate electronically by following the instructions given at the conclusion of the activity.

CME/MOC/ECME Objective for This Article: Upon completion of this activity, the learner should be able to: 1) establish a diagnostic algorithm for the assessment of an "abnormal" right ventricle (RV); 2) identify different types of RV adaptation to abnormal loading conditions and myocardial disease; 3) identify similarities and dissimilarities between the RV and left ventricle; 4) recognize the importance of adequate RV-pulmonary artery coupling; and 5) identify common etiologies of RV cardiomyopathy.

CME/MOC/ECME Editor Disclosure: *JACC* CME/MOC/ECME Editor Ragavendra R. Baliga, MD, FACC, has reported that he has no financial relationships or interests to disclose.

Author Disclosures: The authors have reported that they have no relationships relevant to the contents of this paper to disclose.

Medium of Participation: Print (article only); online (article and quiz).

CME/MOC/ECME Term of Approval

Issue Date: April 2, 2019
Expiration Date: April 1, 2020

Listen to this manuscript's audio summary by Editor-in-Chief Dr. Valentin Fuster on JACC.org.

From the [a]Icahn School of Medicine at Mount Sinai, New York, New York; [b]Centro Nacional de Investigaciones Cardiovasculares Carlos III (CNIC), Madrid, Spain; [c]Department of Anatomy and Cell Biology, Faculty of Medicine, University of Extremadura, Badajoz, Spain; [d]Cardiology Division, "A. Cardarelli" Hospital, Naples, Italy; [e]Amsterdam UMC, Vrije Universiteit Amsterdam, Department of Pulmonary Medicine, Cardiovascular Sciences, Amsterdam, the Netherlands; and the [f]Department of Pathophysiology, Faculty of Medicine, Université Libre de Bruxelles, Brussels, Belgium. The authors have reported that they have no relationships relevant to the contents of this paper to disclose. Marvin A. Konstam, MD, served as Guest Editor for this paper.

Manuscript received October 2, 2018; revised manuscript received December 12, 2018, accepted December 22, 2018.

ISSN 0735-1097/$36.00 https://doi.org/10.1016/j.jacc.2018.12.076

JACC VOL. 73, NO. 12, 2019
APRIL 2, 2019:1463–82

Anatomy, Function, and Dysfunction of the Right Ventricle

JACC State-of-the-Art Review

Javier Sanz, MD,[a,b] Damián Sánchez-Quintana, MD, PhD,[c] Eduardo Bossone, MD, PhD,[d] Harm J. Bogaard, MD, PhD,[e] Robert Naeije, MD, PhD[f]

ABSTRACT

There is increasing recognition of the crucial role of the right ventricle (RV) in determining functional status and prognosis in multiple conditions. The normal RV is anatomically and functionally different from the left ventricle, which precludes direct extrapolation of our knowledge of left-sided physiopathology to the right heart. RV adaptation is largely determined by the level of exposure to hemodynamic overload (both preload and afterload) as well as its intrinsic contractile function. These 3 processes (pressure overload, volume overload, and RV cardiomyopathy) are associated with distinct clinical course and therapeutic approach, although in reality they often coexist in various degrees. The close relationship between the RV and left ventricle (ventricular interdependence) and its coupling to the pulmonary circulation further modulate RV behavior in different clinical scenarios. In this review, the authors summarize current knowledge of RV anatomic, structural, metabolic, functional, and hemodynamic characteristics in both health and disease.
(J Am Coll Cardiol 2019;73:1463–82)

In 1943, after severely damaging the free wall of the right ventricle (RV) with a "red-hot soldering iron," Starr et al. (1) noted only minimal increases in peripheral venous pressure. This and similar experiments led to the conclusion that "a normal, contractile right ventricular wall is not necessary for the maintenance of a normal circulation" (2), a concept further validated by completely excluding the RV in patients (Fontan circulation) (3). As a result, the importance of the RV was neglected for decades. However, new impetus in understanding the RV in health and disease has emerged from accumulating evidence of its almost universal clinical relevance, both from symptomatic and prognostic perspectives, in scenarios such as ischemic and nonischemic heart failure (with either reduced or preserved ejection fraction [EF]), myocardial infarction, pulmonary hypertension (PH), congenital heart disease, or after therapeutic interventions (4).

When a clinician faces an "abnormal RV," the main considerations are to determine whether the chief underlying process is pressure overload, volume overload, or a primary myocardial process (**Central Illustration, Table 1**), because the clinical course and therapeutic approach in these 3 situations differ significantly. This review is thus divided into 4 sections: the normal RV, the pressure-overloaded RV, the volume-overloaded RV, and the cardiomyopathic RV. Nevertheless, it must be realized that this classification, although useful from a clinical perspective, is necessarily artificial, because different processes frequently coexist. Furthermore, there is a continuum between health and disease, and an intimate relationship between preload and afterload so that the 2 cannot be easily dissociated. A detailed review of techniques for RV assessment is beyond the scope of this paper; an overview of different approaches is presented in **Table 2**.

THE NORMAL RV

NORMAL ANATOMY, MYOARCHITECTURE, AND EMBRYOLOGY. The RV in mammals and in birds is a thin-walled crescent-shaped structure coupled to systemic venous return on one side and to the pulmonary circulation on the other. It is 10% to 15% larger in volume than the left ventricle (LV) with a thinner free wall (3 to 5 mm in the adult) and one-third to one-sixth smaller mass (5,6). When imaging the RV, it can be divided into anterior, lateral, and inferior walls, as well as basal, mid, and apical segments (7). From an anatomic standpoint, the RV is more often described in terms of 3 components (**Figure 1**): 1) the inlet, which consists of the tricuspid valve, tendinous chords, and 3 or more papillary muscles; 2) the trabeculated apex, often very thin (which may make this portion more susceptible to increased wall stress); and 3) the outlet or infundibulum (conus), a tubular muscular structure that supports the pulmonary valve leaflets. The size of the

HIGHLIGHTS

- Anatomically and functionally different from the left ventricle, the RV plays an increasingly recognized role in determining symptoms and outcomes in multiple conditions.
- The normal RV is coupled to the low-pressure, high-compliance pulmonary circulation to ensure transfer of blood to the pulmonary arteries in an energy efficient fashion. RV adaptation to disease is determined by the degree of pressure overload, volume overload, and alterations in intrinsic contractility, 3 situations with distinct clinical course and therapeutic approach although commonly coexisting in various degrees.
- Refinements in the evaluation of RV anatomy, myoarchitecture, ultrastructure, metabolism, perfusion, and function, and of its degree of coupling (or lack thereof) to the pulmonary circulation, either invasively or increasingly through noninvasive imaging, promise to enhance our understanding of the mechanisms of RV adaptation or maladaptation to pathologic conditions.

ABBREVIATIONS AND ACRONYMS

Ea = arterial elastance
EDV = end-diastolic volume
Ees = end-systolic elastance
EF = ejection fraction
ESV = end-systolic volume
LV = left ventricle
PA = pulmonary artery
PH = pulmonary hypertension
RV = right ventricle
SV = stroke volume

infundibulum is independent of the general size of the RV, and accounts for approximately 20% of end-diastolic volume (EDV) in the normal RV (8). The crista supraventricularis, supraventricular crest, or ventriculoinfundibular fold separates the RV inlet (tricuspid valve) and outlet (pulmonary valve) components (**Figure 1**). The crista continues as a parietal band in the RV free wall and as the septomarginal or septal band in the septum, and when shortening, it contracts the tricuspid annulus and pulls the free wall toward the septum (4). The septomarginal band is a prominent Y-shaped muscular strap that, when hypertrophied or abnormally formed, can divide the RV into 2 chambers (double-chambered RV) (9). The inferior limb of the septal band becomes continuous with the moderator band, to which the anterior papillary muscle attaches (**Figure 1**). The moderator band incorporates the right bundle branch of His and frequently collaterals from the first septal, and can be identified in 90% of hearts (10). The RV is morphologically and functionally distinct from the LV. Distinguishing characteristics of the morphological RV include uniformly coarse trabeculations (in fact the most constant anatomical feature for the cardiac morphologist), multiple papillary muscles, the moderator band, a tri-leaflet atrioventricular valve with a septal leaflet that is apically displaced compared with the anterior mitral leaflet, and a fully muscular outflow tract (as opposed to the aortomitral continuity of the LV).

There are individual variations from heart to heart, but in general, the myoarchitecture conforms to some constant muscular patterns. In the LV there are 3 distinct myocardial "layers" of aggregated cardiomyocytes; however, no proper middle "layer" can be defined in the RV. The superficial layer (approximately 25% of wall thickness) is formed by predominantly circumferential aggregates in a direction parallel to the atrioventricular groove that extend from one ventricle to another (**Figure 2A**). In the RV, myocytes in this layer are arranged more circumferentially than in the LV. The subendocardial RV layer is composed of preferentially arranged longitudinal myocytes that pass through the apex toward the papillary muscles, tricuspid annulus, and RV outflow tract (**Figure 2B**) and are continuous with those of the septum. The RV and LV are closely inter-related not only through the septum but also shared epicardial circumferential myocytes and the pericardial space, all of which constitute the anatomic basis for biventricular functional systolic and diastolic interdependence (11).

Disparities between the RV and LV arise from differences in embryological origins as well as hemodynamic environment. The morphogenesis of the cardiovascular system begins at around 3 weeks of gestation and is mostly completed by 8 weeks in humans. Cells derived from the anterior lateral plate mesoderm coalesce along the ventral midline to form a primitive heart tube. The "first" heart field that forms the heart tube eventually contributes to specific future chambers: LV, muscular interventricular septum, and atria. The future RV, most of the membranous interventricular septum, and outflow tracts derive from cardiac precursors cells in the anterior or "second" heart field (12). In the embryo and fetus, the RV is the dominant chamber accounting for about 60% of total cardiac output, and during fetal development the wall thickness and forces generated by the RV and LV are equal (13). At birth, pulmonary vascular resistance decreases rapidly, and by the first postnatal year, RV wall thickness regresses, increasing compliance and leading to normal cardiac morphology with rightward septal convexity (**Central Illustration**).

CENTRAL ILLUSTRATION **The Right Ventricle: Anatomy, Function, and Dysfunction**

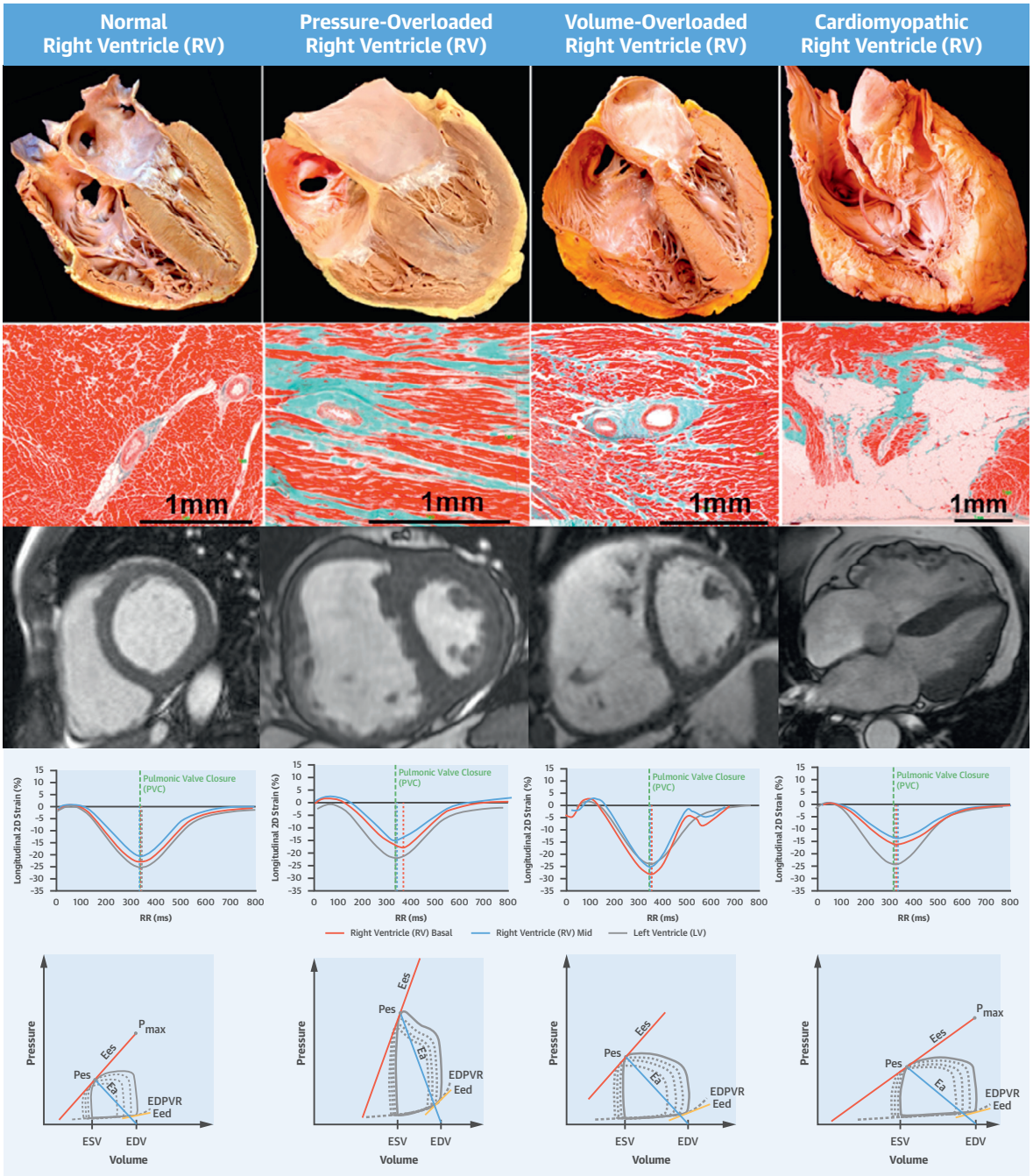

Sanz, J. et al. J Am Coll Cardiol. 2019;73(12):1463–82.

Overview of pathology, histology, magnetic resonance, echocardiography-based strain, and pressure-volume loop findings in the RV in health and disease. The pressure overloaded RV demonstrates hypertrophy and dilatation, systolic septal flattening, extensive fibrosis, reduced myocardial deformation with dyssynchrony and post-systolic shortening, and highest increases in end-systolic (Ees), end-diastolic (Eed), and arterial (Ea) elastances. The volume overloaded RV demonstrates dilatation, diastolic septal flattening, mild fibrosis, near-normal and synchronous myocardial deformation, and preserved coupling. The cardiomyopathic RV (arrhythmogenic cardiomyopathy in the figure) demonstrates RV dilatation and aneurysms, fibrofatty replacement, severely reduced myocardial strain, and decreased Ees. 2D = 2-dimensional; EDPVR = end-diastolic pressure-volume relationship; EDV = end-diastolic volume; ESV = end-systolic volume; LV = left ventricle; Pes = end-systolic pressure; PVC = pulmonic valve closure; RV = right ventricular.

TABLE 1 Etiologies of RV Pressure Overload, Volume Overload, and RV Cardiomyopathy

RV Pressure Overload	RV Volume Overload	RV Cardiomyopathy
Pulmonary hypertension*	Valvular regurgitation	Myocardial infarction
Pulmonary arterial hypertension	Tricuspid	ARVC
Due to left heart disease	Pulmonary	Dilated cardiomyopathy
Due to lung disease and/or hypoxia	Systemic-to-pulmonary shunt	Hypertrophic cardiomyopathy
CTEPH and other pulmonary artery obstructions	Atrial septal defect	Amyloidosis
Unclear and/or multifactorial mechanisms	Partial anomalous pulmonary vein drainage	Myocarditis
Pulmonary valve stenosis	High output states† (i.e., thyrotoxicosis)	Sarcoid
Pulmonary artery stenosis		Transplant
Pulmonary embolism		Post-surgery
		Post-LVAD
		Cardiotoxicity (i.e., chemotherapy)
		Sepsis

*Main groups according to the European Society of Cardiology Classification. †Concomitant left ventricular volume overload.

ARVC = arrhythmogenic right ventricular cardiomyopathy; CETPH = chronic thromboembolic pulmonary hypertension; LVAD = left ventricular assist device; PAPVD = partial anomalous pulmonary vein drainage.

NORMAL STRUCTURE, METABOLISM, AND PERFUSION. It is well established that human RV cardiomyocytes are about 15% smaller than LV cardiomyocytes (14). Interestingly, despite higher compliance and probably because of smaller myocyte size, the RV contains 30% more collagen (15). Potential differences in gene and protein expression between LV and RV cardiomyocytes have been little studied. Proteomic and transcriptomic studies suggest that mammalian RV and LV cardiomyocytes have a large overlap in gene expression and very similar protein composition (16,17). As such, it is safe to assume that the processes of excitation and contraction are quite similar in RV and LV cardiomyocytes. There are no human studies on changes in cardiomyocyte composition or function with increasing age; however, animal models indicate myocyte loss, abnormalities in calcium handling, and reductions in contractility (18). Imaging studies have demonstrated lower RV mass and EDV and higher EF (albeit with reduced deformation) with aging, perhaps as a compensatory response to myocyte loss and pulmonary artery (PA) stiffening (19). Reductions in RV volume and myocyte replacement with connective tissue may contribute to impaired RV diastolic filling in the elderly (20). Although cellular and molecular studies comparing the human male and female RV are lacking altogether, RV volumes and mass tend to be higher in men, whereas RV EF is lower (19). This may be related to cardioprotective effects of estrogens, as supported by both observational and experimental studies (21,22).

There are also no convincing data to suggest that the energy source for contraction in the RV is different from the LV (23). In the normal adult heart, fatty acid oxidation is the predominant source of adenosine-triphosphate production (60% to 90%), with glucose metabolism generating the remainder. Oxidative metabolism consumes oxygen but yields much more adenosine-triphosphate than cytoplasmic (anaerobic) glycolysis (24). RV-LV comparative studies in humans are difficult to perform because of the inaccessibility of the normal thin-walled RV to metabolic imaging. In a rodent model, expression of anaerobic glycolytic enzymes appeared higher in RV than LV cardiomyocytes (25), which could partly explain the relative RV resistance to ischemia. The blood supply of the RV has distinctive features in comparison to the LV (26). Resting coronary blood flow and conductance are lower in the RV, and coronary flow occurs both in systole and diastole. Because of thinner wall and higher dependence on coronary perfusion pressure, RV perfusion is more vulnerable to increases in RV cavitary (and thus intramural) pressure and to systemic hypotension. Oxygen consumption and extraction at rest are also lower than in the LV, resulting in higher oxygen extraction reserve. There is evidence to suggest that pressure-flow autoregulation is somewhat impaired, so the RV increases oxygen consumption during exercise through increased oxygen extraction rather than coronary flow (26).

NORMAL FUNCTION. The RV contracts in a highly synchronized fashion that occurs 20 to 50 ms earlier in the sinus and apex than the conus, resulting in a peristalsis-like motion (5,8,27). The conus may serve as a buffer against high systolic pressures being transmitted to the PA due to its late contraction, higher curvature, and possibly greater inotropic response (5,7). Helical flow developed in the outflow may also contribute to better flow stability into the PA

TABLE 2 Summary of Invasive and Noninvasive Modalities for RV Assessment and Their Measured Parameters

Invasive	
Right heart catheterization	
Contrast ventriculography	End-diastolic volume, end-systolic volume, stroke volume, ejection fraction, regional wall motion
Standard catheterization	End-diastolic pressure, peak systolic pressure
Thermodilution	Cardiac output, stroke volume
High-fidelity micromanometer	dp/dt
Conductance catheter	End-systolic elastance, arterial elastance, end-diastolic elastance, stiffness constant β, stroke work, preload recruitable stroke work, RV power
Intracardiac echocardiography	Dimensions and function
Noninvasive	
Ultrasound	
M-mode	TAPSE, diameters, wall thickness, right atrial size
2D	Fractional area change, eccentricity index, wall thickness, regional wall motion, right atrial size Speckle tracking: myocardial strain, strain rate, dyssynchrony
3D	End-diastolic volume, end-systolic volume, stroke volume, ejection fraction, wall thickness, regional wall motion, right atrial size Speckle tracking: myocardial strain, strain rate, dyssynchrony
Doppler	E, A, deceleration time, isovolumic relaxation time, myocardial performance index, dp/dt, stroke volume Tissue Doppler: E′, A′, E/E′, S′, myocardial performance index, peak isovolumic velocity, isovolumic acceleration, strain, strain rate, dyssynchrony
Contrast	Intraventricular flow patterns, vorticity
Magnetic resonance imaging	
Cine	End-diastolic volume, end-systolic volume, stroke volume, ejection fraction, mass, regional wall motion, right atrial size Feature tracking: strain, strain rate, dyssynchrony
Tagging	Strain
Strain encoded imaging (SENC)	Strain
Phase contrast	Stroke volume, cardiac output, myocardial velocity
Contrast first-pass imaging	Myocardial perfusion
T2-weighted imaging	Myocardial edema
Late gadolinium enhancement	Fibrosis/necrosis
T1-mapping	Native T_1, ECV
Computed tomography	
Noncontrast	Myocardial fatty infiltration
Contrast-enhanced*	End-diastolic volume, end-systolic volume, stroke volume, ejection fraction, mass, wall thickness, regional wall motion, right atrial size
Nuclear imaging	
First-pass radionuclide angiography	End-diastolic volume, end-systolic volume, stroke volume, ejection fraction
Equilibrium radionuclide angiography	End-diastolic volume, end-systolic volume, stroke volume, ejection fraction
SPECT	
99TC-tracers	End-diastolic volume, end-systolic volume, stroke volume, ejection fraction, perfusion
BMIPP	Fatty acid metabolism
PET	
^{18}F-FDG	Glucose metabolism
^{11}C-palmitate	Fatty acid metabolism
^{18}F-FTHA	Fatty acid metabolism
^{11}C-acetate	Oxygen consumption
$^{15}O_2$-tracers	Oxygen consumption
Cardiopulmonary exercise test	Peak oxygen consumption, minute ventilation, ventilatory efficiency, oxygen pulse

*Retrospective ECG gating.

2D = 2-dimensional; 3D = 3-dimensional; BMIPP = ^{123}I beta-methyl-p-iodophenyl-pentadecanoic acid; ECV = extracellular volume; FDG = fluorodeoxyglucose; FTHA = fluoro-6-thioheptadecanoic acid; PET = positron emission tomography; SPECT = single photon emission computed tomography; TAPSE = tricuspid annular plane systolic excursion.

(28). Most (although not all) studies have suggested that apical EF is smaller compared with the inlet and outlet regions (27,29,30). Early data suggest that, in contrast with the vortex-dominated flow organization of the LV, direct flow patterns within the RV are relatively streamlined following a smooth curved path from the inflow to the outflow along the septum, largely circumventing the apex (28,31) (**Figure 3**). This

is considered a direct consequence of the peculiar RV shape and in line with its low pressure levels, so that little help is required for flow redirecting as opposed to the systemic circulation. These findings also suggest that the role of the apex may be maintaining a smooth and continuous blood flow rather than contributing to ejection (27,31). Probably because of the previously mentioned predominance of longitudinal subendocardial myocytes, longitudinal shortening accounts for approximately 75% of RV contraction (32). Regarding regional RV function, although results have varied somewhat across reports, likely because of different endpoints and techniques, most have indicated decreasing free wall velocities from base to apex but higher apical deformation (7,33–35).

The LV is an important contributor to RV ejection: in experimental models, LV contraction generates 20% to 40% of both RV stroke volume (SV) and pulmonary flow (4,23). This is largely mediated through septal contraction, although other contributory mechanisms exist (11,36). Conversely, the RV is also important in maintaining cardiac output, particularly during exercise, as shown indirectly by a 30% to 50% decrease in predicted maximum oxygen uptake in healthy Fontan patients (37). The quality of the RV is not in generating pressure, but rather in streamlining varying amounts of venous return into a relatively constant SV that is ejected into the low-impedance pulmonary circulation with one-fourth of the LV stroke work (5). The thinner wall and lower volume-to-wall-surface area ratio render the RV more compliant and capable of accommodating increased preload, but unable to cope with brisk increments in PA pressures. An acute increase of either preload or afterload is immediately associated with RV dilatation to preserve SV. After several minutes, this "heterometric" adaptation is replaced by an "homeometric" adaptation with normalization of EDV and increased contractility. In spite of embryological and structural differences, RV and LV homeometric and heterometric adaptations to changes in loading conditions are basically the same (38).

Although RV preload is easily defined as EDV (the moment of maximal stretch of myocardial fibers before isovolumic contraction), there are several valid but conceptually different definitions of RV afterload (23). The first is maximum wall tension, which is directly proportional to volume and pressure and inversely to wall thickness as determined by Laplace's law for spherical structures. This may be considered the reference definition of afterload, but it is difficult to apply to the RV because of its irregular shape and inhomogeneous contraction. Another is external RV work or power, the energy lost by the RV as blood flows through the pulmonary circulation, calculated as SV times PA pressure. Impedance or hydraulic load comprises all of the forces that oppose RV flow output. This is calculated from the integration of instantaneous PA pressure and flow waves, but is unstable, prone to errors, and of limited availability. Finally, afterload can be measured as arterial elastance (Ea). Elastance, the change in pressure for a given change in volume, is a property that describes an elastic chamber. Ea can be obtained from RV pressure-volume loops (**Figure 4**) as RV end-systolic pressure divided by SV. Mean PA pressure is a reasonable approximation of end-systolic pressure in the normal RV so that Ea can be calculated as mean PA pressure divided by SV, or as pulmonary vascular resistance multiplied by heart rate (39). Maximum elastance is the gold standard estimate of contractility and takes place a bit before end-systole in the normal RV, but at end-systole in the presence of PH.

FIGURE 1 Window Dissection of a Heart

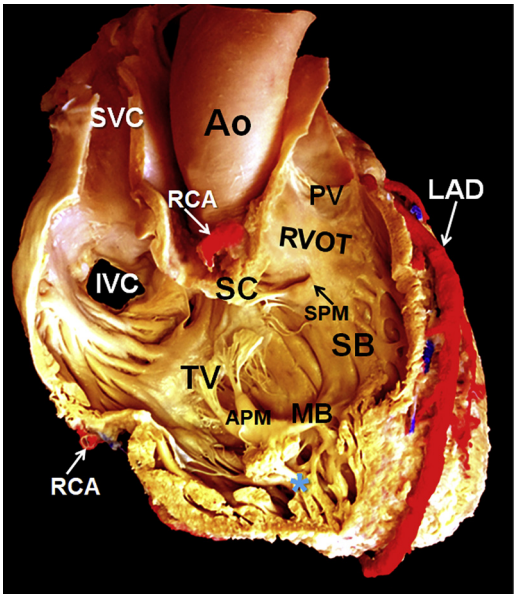

Window dissection of a heart prepared by removing the anterior superior wall of the RV, revealing the inlet (TV), trabecular apex (*), and RVOT or infundibulum. Ao = aorta; APM = anterior papillary muscle; IVC = inferior vena cava; LAD = left anterior descending artery; MB = moderator band; PA = pulmonary artery; PV = pulmonary valve; RCA = right coronary artery; RV = right ventricle; RVOT = right ventricular outflow tract; SB = septomarginal or septal band; SC = supraventricular crest; SPM = septal papillary muscle; SVC = superior vena cava; TV = tricuspid valve.

FIGURE 2 RV Myoarchitecture

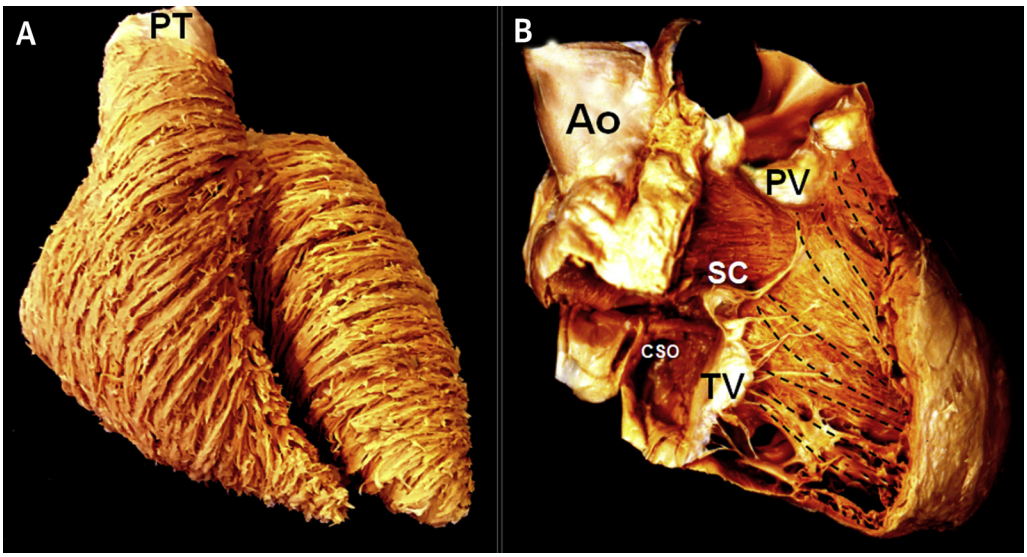

(A) Normal heart viewed from the front shows the circumferential arrangement of superficial RV and middle LV layers of aggregated cardiomyocytes. **(B)** Opened normal RV showing longitudinally arranged subendocardial myocyte aggregates **(black dashed lines).** CSO = coronary sinus ostium; LV = left ventricle; PT = pulmonary trunk; other abbreviations as in Figure 1.

Thus, RV end-systolic elastance (Ees) is generally an acceptable approximation for maximum elastance (5) and is calculated from invasive pressure-volume loops as end-systolic pressure (or mean PA pressure) divided by end-systolic volume (ESV) (**Figure 4**). Diastolic function can be also described from invasive pressure-volume curves as diastolic stiffness constant β or end-diastolic elastance (**Figure 4**) (39,40).

NORMAL VENTRICULOARTERIAL COUPLING. The comparison of Ea and Ees allows determination of the adequacy of RV contractility adaptation to afterload or "coupling" between the RV and the pulmonary circulation, also termed right heart-pulmonary circulation unit (41). Optimal ventriculoarterial coupling takes place when there is maximal transference of potential energy from one elastic chamber (the ventricle) to another (the arterial system), and this occurs if both elastances are equal (Ees/Ea = 1). However, the optimal Ees/Ea ratio for ejection at minimal energy cost, as seen in the normal RV, is 1.5 to 2.0 (23,38). Measurements of Ees and Ea can be obtained from a family of pressure-volume loops at several levels of preload (42) or from single-beat ventricular pressure and flow output measurements (43) (**Figure 4**). The single-beat method avoids technically demanding measurements at variable levels of loading and of absolute RV volumes; nonetheless, both present technical and logistical challenges, and simplified approaches have been developed (38). The single-beat method can be reduced to a ratio of pressures, easy to obtain during a standard right heart catheterization (44). Similarly, because both Ees and Ea have a common pressure term, coupling can be simplified as SV/ESV, quantifiable with magnetic resonance (45). The volume method is intimately related to EF, the latter also an index of ventriculoarterial coupling rather than RV contractility (46). Both simplified methods rely on assumptions that may not be equally true in all circumstances (38,39), so further validation is required. There has also been recent interest in the estimation of ventriculoarterial coupling by a ratio between tricuspid annular plane excursion (as a surrogate of contractility) and systolic PA pressure (as a surrogate of afterload). This correlates with Ees/Ea but not tightly (47), so more studies are needed to better understand its significance.

THE PRESSURE-OVERLOADED RV

RV ANATOMY IN PRESSURE OVERLOAD. RV pressure overload, most commonly secondary to PH, leads to RV hypertrophy, predominantly end-systolic and early-diastolic flattening of the interventricular septum, and eventually, progressive RV dilation and

dysfunction (**Central Illustration**). Myocyte hypertrophy and disarray (**Figure 5**) involve not only the compacted RV wall but also the trabeculations and muscular bands (48). A prominent septoparietal band containing circumferentially aligned or crisscrossed aggregated cardiomyocytes may contribute to muscular subpulmonary stenosis (49). Although studies in congenital heart disease (50) or some experimental models (51) suggest a more circumferential orientation of myocyte aggregates, others have found overall preserved RV structure (52) or predominantly longitudinal reorientation (53), so it is uncertain if RV pressure overload leads to predictable changes in myoarchitecture. Interestingly, pressure overload is better tolerated in the setting of congenital heart disease (pulmonary valve stenosis, Eisenmenger), probably because of absence of RV hypertrophy regression after birth and persistence of a "fetal" phenotype (54).

RV STRUCTURE, METABOLISM, AND PERFUSION IN PRESSURE OVERLOAD. It has become apparent that the adaptive capacity of the RV is immense and in fact is much larger than that of the LV. In PH, the RV may face a 5-fold rise in afterload, which is much greater than the approximately 50% increase in systemic hypertension or aortic stenosis. The first step in RV adaptation is through mechanotransduction, the intrinsic ability of cardiomyocytes to sense and respond to load through conformational changes in integrins, stretch-activated ion-channels, and the major sarcomeric protein titin (55). However, trophic paracrine signals from stretched cardiac fibroblasts may be equally important (56). While in many circumstances LV hypertrophy is considered a maladaptive response, successful RV adaptation without hypertrophy is unthinkable. Cardiomyocyte hypertrophy occurs through accumulation of sarcomeric proteins, usually accompanied by the re-emergence of a fetal gene expression pattern such as increased expression of natriuretic peptides and a switch from α-myosin to β-myosin heavy chain that exhibits reduced energy requirements but also contractility (57). In contrast to LV hypertrophy, fetal gene expression does not discriminate between adaptive and maladaptive stages of RV hypertrophy (16). As in LV failure, a clear distinction between "good" and "bad" molecular adaptation is difficult to make. The pivotal pathobiological hallmarks of heart failure, such as neurohormonal activation and impaired calcium handling, are definitively seen in both RV and LV failure (57).

Hypertrophy of tissue increases oxygen demand and requires a proportional increase in blood supply, a process in which angiogenesis driven by the hypoxia inducible factor-1α/vascular endothelial growth factor axis plays a pivotal role. Indeed, blocking the latter interferes with normal cardiac adaptation to

FIGURE 3 3-Dimensional Representation of Helical Streamlines of Normal RV Intracavitary Flow During Systole

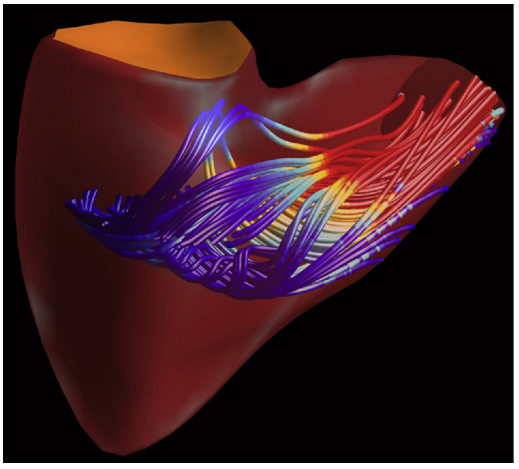

Reprinted with permission from Sengupta and Narula (28).

FIGURE 4 Multiple-Beat and Single-Beat Methods for Calculating Ea and RV Ees

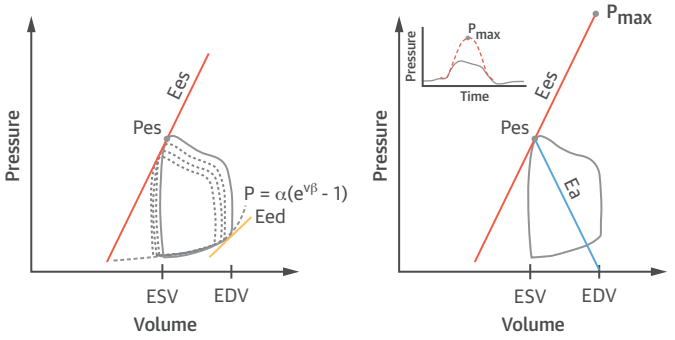

(Left) Multiple beat method; **(right)** single-beat method. In both methods, arterial elastance (Ea) is calculated from the ratio of end-systolic pressure (ESP) to stroke volume (**slope of the line** connecting end-systolic [ESV] and end-diastolic volumes [EDV]). End-systolic elastance (Ees) is estimated by the ratio of ESP to ESV. In the multiple-beat method, different pressure-volume curves are generated by changing preload, and Ees is calculated from the **slope of the line** connecting end-systolic pressure-volume relationships. In the single-beat method, maximal RV pressure ([Pmax] or maximal pressure generated during an isovolumic contraction), is estimated from the nonlinear extrapolation of the early systolic and diastolic portions of the RV pressure curve. Ees is calculated from the **slope of a straight line** from Pmax tangent to the RV end-systolic pressure-volume relationship (or Pmax-ESP/stroke volume). Diastolic stiffness constant β is calculated by fitting the nonlinear exponential curve through the origin as well as early and late end-diastolic pressure-volume relationships, where P is pressure, α is a curve-fitting constant, and V is volume. End-diastolic elastance (Eed) is calculated as the slope of the pressure-volume relationship at end-diastole.

FIGURE 5 Histological Sections With Masson's Trichrome Staining of Normal Pig RV Myocardium and After 4 Months of Pulmonary Vein Banding

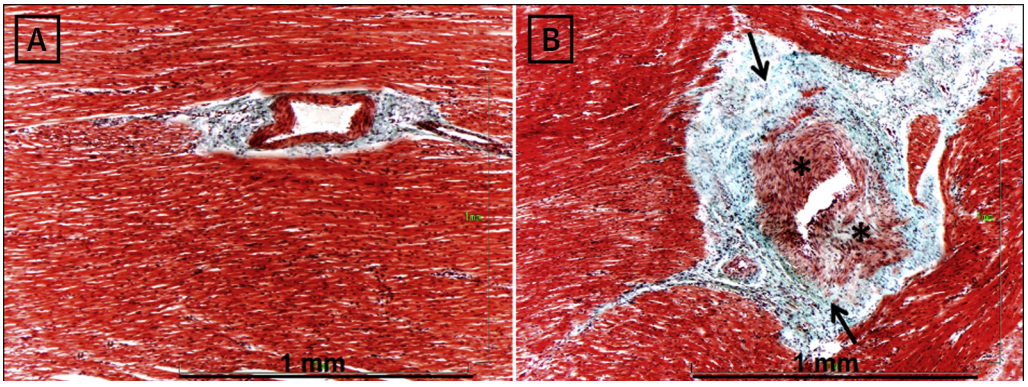

(A) Normal pig right ventricular (RV) myocardium, and **(B)** after 4 months of pulmonary vein banding. In experimental pulmonary hypertension, there is cardiomyocyte hypertrophy and disarray, arterial medial hypertrophy **(*)**, and lymphocytic infiltration with collagen deposition around blood vessels **(arrows).**

pressure overload (58). While an oxygen supply-demand imbalance has certainly been demonstrated in patients with PH-associated right heart failure (59), it is still unclear whether this is related to a global reduced perfusion and/or to capillary rarefaction. Several groups have shown a loss of capillaries in the failing RV of rats (60), but these findings could not be confirmed using stereological quantifications (61). Several other mechanisms could explain impaired perfusion of the failing RV, such as systemic hypotension, impairment of systolic coronary flow in the setting of increased wall stress, mechanical inefficiency, and compression of the right coronary artery by a dilated PA (36,39,62).

Another possible consequence of impaired oxygen supply is metabolic remodeling. Proteomic studies in the rat have shown decrease in beta-oxidation enzymes and increase in anaerobic glycolytic enzymes (63), suggesting a "metabolic switch" from mitochondrial-based fatty acid oxidation to less efficient but oxygen-sparing anaerobic glycolysis as preferred energy source. Autopsy human studies have also confirmed increased expression of anaerobic glycolytic enzymes in the pressure overloaded RV (64). Imaging in PH patients has shown large increases in RV glucose uptake (65); however, to what extent this is secondary to a true metabolic shift or to increased stroke work or ischemia is uncertain. Data on RV fatty acid uptake have been controversial (23). Experimental studies suggest that the transition from adaptive to maladaptive RV hypertrophy is characterized by an ultimate decline in glucose uptake and glycolysis, favoring the development of RV ischemia (66). This has not been confirmed in the human heart and is currently debated (24). RV function in the setting of pressure overload is better preserved in women, and a proposed explanation is predominant expression of genes related to mitochondrial function in women but to matrix biosynthesis in men (67).

Although macroscopic RV infarcts are rare in PH, short episodes of ischemia could definitively be responsible for the development of RV fibrosis (**Figure 5**). Numerous studies have shown RV myocardial fibrosis and its relevance in experimental PH (68,69). The suggestion that it may be present in human RV pressure overload comes from histological (40) and magnetic resonance studies (70). Interestingly, Eisenmenger hearts display less fibrosis than those with idiopathic PH, again suggesting better adaptation (71). If fibrosis develops, this seems to be much less than in the pressure-overloaded LV, which may explain why most patients recover RV function after lung transplantation (72). Nevertheless, autopsy data regarding RV fibrosis in pressure overload have not been consistent (23). The same is true for cardiac inflammation (**Figure 5**), which could also result from recurrent boots of RV ischemia. Although influx of inflammatory cells into the RV has been demonstrated in acute RV failure due to massive pulmonary embolism, there is little data on the possible role of inflammation in the development of RV failure in pressure overload (73).

FIGURE 6 **RV Function Response to a Progressive Increase in PVR in Pulmonary Hypertension**

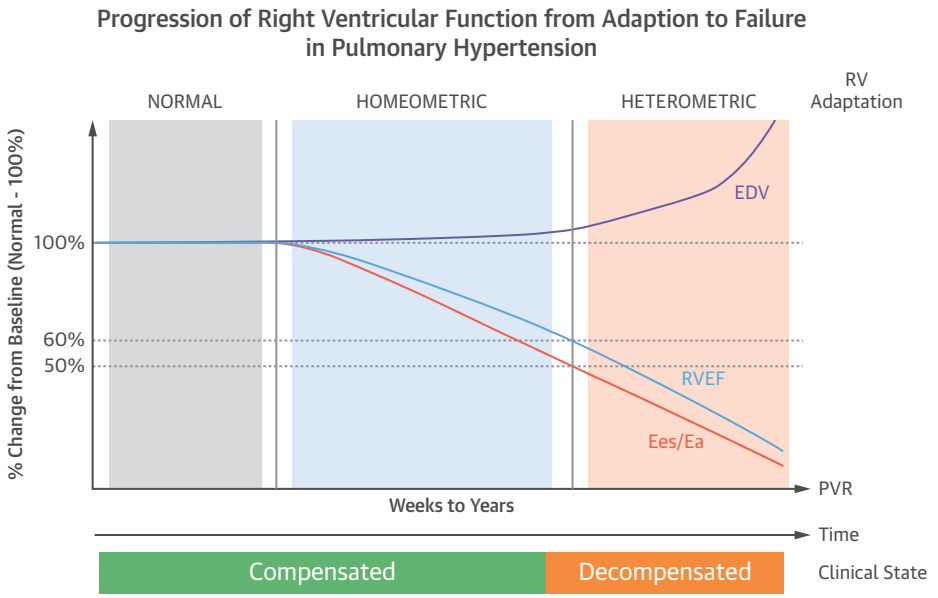

During the adapted "homeometric" phase, contractility increases to maintain the Ees to Ea ratio (Ees/Ea) but does so insufficiently, so that the Ees/Ea progressively declines along with an almost parallel decrease in ejection fraction (EF). Ees/Ea and EF have to decrease, respectively, by >50% and 40% (corresponding to Ees/Ea <0.7 to 0.8 and EF <35%) before heterometric adaptation (Starling's law) is turned on, with rapid progressive increase in EDV and poor prognosis. PVR = pulmonary vascular resistance; other abbreviations as in **Figures 1 and 4**.

RV FUNCTION IN PRESSURE OVERLOAD. In the setting of chronic pressure overload, the RV initially responds with "adaptive" remodeling characterized by relatively preserved volumes and function and compensatory "concentric" hypertrophy (increased mass to volume ratio that decreases wall tension). This corresponds to a stage where functional status, exercise capacity, and cardiac output may remain reasonably well preserved. When this homeometric adaptation gets exhausted and contractility can no longer increase to match afterload, "maladaptive" remodeling takes place with "eccentric" hypertrophy, progressive RV dilatation and dyssynchrony, and maintenance of SV through Frank-Starling mechanisms (heterometric adaptation). This comes at the price of increased filling pressures and, eventually, clinical decompensation (23,72) (**Figure 6**). Imaging RV dimensions thus becomes essential to the diagnosis and prognostication of right heart failure.

Abnormalities in RV systolic function are often present at rest, but exercise may additionally reveal reduced reserve as well as borderline or latent ventriculoarterial uncoupling and pending right heart failure (74,75). As PH progresses, the RV becomes less dependent on longitudinal shortening and more on transverse wall motion (32,35). Myocardial deformation and EF are preferentially reduced in the apex (27,30,33–35), even when global function appears preserved (29). An important component of RV contractile dysfunction in pressure overload is dyssynchrony. Intraventricular RV dyssynchrony may be present in early disease stages (76), leads to loss of peristaltic motion (27) and heterogeneous increases in RV free wall workload (77), and is associated with clinical worsening (78). In addition, interventricular dyssynchrony (delay of RV free wall peak shortening compared to the septum or LV free wall) occurs in more advanced stages. RV contraction is prolonged in PH and may extend past pulmonary valve closure (post-systolic isovolumic contraction), contributing to increased wall stress and mechanical inefficiency (39). This prolonged contraction is a major determinant of interventricular dyssynchrony and leftward septal shift, which leads to LV underfilling and subsequent reduction in SV (79). Eventual RV dilatation causes additional deleterious ventricular interaction in diastole (see section on the volume-overloaded RV). For these reasons, knowledge of both RV dimensions and function is relevant in PH. RV pressure overload is also associated with RV diastolic

FIGURE 7 Ventricular Volumes at Decreasing RV Ejection Fraction or SV to ESV Ratio

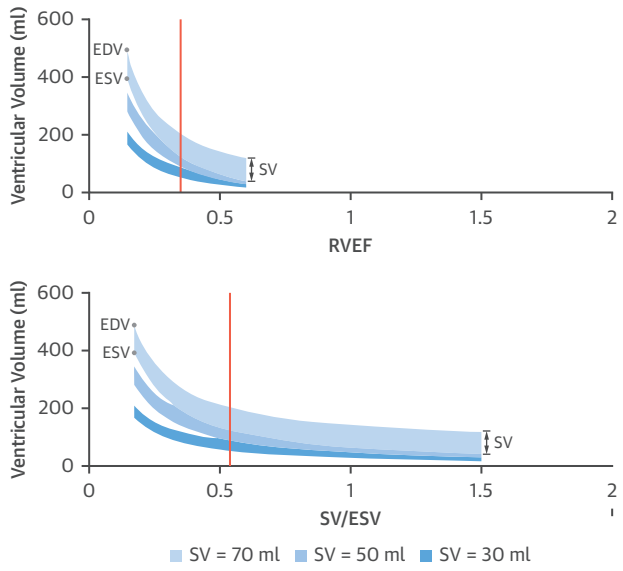

The **vertical lines** show cut-off values of 0.35 and 0.54, respectively, below which EDV and ESV must increase for SV preservation. Reproduced with permission from Naeije et al. (41). SV = stroke volume; other abbreviations as in Figures 1 and 4.

dysfunction with reduced compliance and relaxation (80), with both cardiomyocyte hypertrophy and fibrosis contributing to increased stiffness (40). Diastolic dysfunction predicts outcomes but is closely related to disease severity and Ees (40,81). Whether diastolic stiffness predicts outcome during RV adaptation or maladaptation to PH independent to Ees remains to be explored.

VENTRICULOARTERIAL COUPLING IN PH. The coupling of the RV to the pulmonary circulation in human PH was first reported in 2004, with single-beat calculation of the Ees/Ea ratio in 6 stable patients and 6 control subjects (82). Ees was approximately doubled but in the face of a quadrupled Ea, so that Ees/Ea was about one-half that of control subjects, implying insufficient contractility and decoupling. Yet, RV volumes were not increased, indicating adequate compensation. The critical levels of decoupling associated with onset of RV dilatation (heterometric adaptation) is not exactly known, but experimental animal observations and measurements in patients have suggested an Ees/Ea ~0.7 at the onset of decreased SV (83). Simplified methods of ventriculoarterial coupling have been used in PH. In chronic pressure overload, the RV pressure-volume loop becomes less trapezoidal and squarer in shape (more "LV-like"). As a result, mean PA pressure underestimates end-systolic pressure in a degree that can be mathematically estimated (84). Compared with the volume method, the pressure method leads to higher Ees/Ea, and appears to better agree with the single-beat approach (44). Nonetheless, the volume method was an independent prognosticator in patients referred for PH, whereas the pressure method and RV EF were not (44). In a different study, both EF and SV/ESV were equally predictive of outcome in pulmonary arterial hypertension (85). The relationship between EF and SV/ESV is nonlinear, so they may have different sensitivity in different disease stages (86). As shown in Figure 7, cutoff values of roughly 0.35 for EF and 0.54 for SV/ESV predict the increase in RV volumes required to maintain SV. Interestingly these cutoffs have been validated as predictors of poor outcome in PH (44,85,87).

Although Ees and Ea are gold standard measures of contractility and afterload, their ratio may not be sensitive to therapeutic interventions, because drugs that decrease afterload will cause a concomitant reduction in contractility to preserve coupling even though RV volumes or EF may improve (88). In severe PH, reverse RV remodeling as defined by reduced RV dimensions and/or increased EF requires decreases in pulmonary vascular resistance of at least 40 to 50% (89,90) (Figure 8).

THE VOLUME-OVERLOADED RV

RV ANATOMY AND STRUCTURE IN VOLUME OVERLOAD. The hallmarks of the volume-overloaded RV are RV dilatation and hypertrophy (increased free wall mass albeit preserved thickness) and predominantly diastolic leftward septal shift (Central Illustration). Because of the anatomic and physiological features discussed previously, volume overload is much better tolerated than pressure overload (4). Although volume overload represents conceptually a predominant increase in preload, RV dilatation leads to augmented wall tension as described earlier, and to an inevitable simultaneous increase in afterload.

The mechanisms of RV adaptation to volume overload have been less extensively studied compared with pressure overload. In feline and murine models, it resulted in a degree of hypertrophy comparable to pressure overload and similar ultrastructural cardiomyocyte changes; conversely, no reductions in myocyte density or increases in β-myosin heavy chain or collagen were noted (91,92). However, in a different mouse model of volume overload secondary to experimentally induced pulmonary insufficiency, there were progressive

increases in RV fibrosis and cardiomyocyte apoptosis (93). Early during volume overload multiple genes were down-regulated, including pathways related to cell metabolism, transmembrane nutrient transport, and calcium signaling, while there was a reactivation of fetal gene programs with increases in β-myosin heavy chain. After 3 months, persistent down-regulation of calcium handling genes and up-regulation of inflammatory pathways via transforming growth factor-β may have contributed, respectively, to contractile dysfunction and increased collagen deposition and extracellular matrix remodeling (93). In addition, there was a late down-regulation of genes involved in beta-oxidation and up-regulation of those needed for glycogenolysis (93), suggesting a metabolic shift similar to that seen in pressure overload. Whether similar changes occur in humans is uncertain. A small study demonstrated increased glucose metabolic rate in the interventricular septum in patients with atrial septal defect, and a similar trend in the RV free wall, without reductions in perfusion or fatty acid uptake (94). Again, whether this reflects a true metabolic shift or simply hypertrophy and/or increased septal contribution to RV ejection is unknown.

RV FUNCTION IN VOLUME OVERLOAD. Experimental studies demonstrate that RV contractility remains preserved in RV volume overload for long periods of time, although contractile reserve may be compromised (95,96). In patients with volume overload, the shape of pressure-volume loops was indistinguishable from that of the normal RV (97). An important consequence of RV volume overload is simultaneous LV dysfunction as evidenced by reduced compliance and EF (11,96). The primary mechanism is underfilling due predominantly to septal displacement and changes in LV geometry, rather than decreased RV forward SV (4). An additional potential mechanism for impaired biventricular systolic performance is the reorientation of myocardial fibers, which could in theory interfere with normal myocardial mechanics (98).

Patterns of RV regional contractility appear to differ according to underlying disease. In patients with atrial septal defect, studies have consistently demonstrated preserved global longitudinal strain in the RV free wall, but supranormal apical strain, suggesting that RV apical contraction contributes significantly to the increased RV output (99,100). However, after surgical correction (even 35 years later) longitudinal strain is reduced, particularly in the apex (100,101). It is uncertain if these residual abnormalities are sequelae of longstanding RV volume overload, surgical intervention, or both (101). Conversely, in the setting of RV volume overload secondary to pulmonary regurgitation in repaired tetralogy of Fallot, there is reduction in RV free wall longitudinal strain that becomes more severe toward the apex (99,101). It needs to be recognized, however, that tetralogy of Fallot represents a unique situation of volume but also, at least prior to repair, pressure overload that may not be extrapolatable to other settings. In fact, these hearts demonstrate an intermediate RV layer of predominantly circumferential myocyte aggregates, hypothesized to be part of the congenital derangement, as opposed to just adaption to increased load (50). In addition, scarring and segmental wall motion abnormalities, consequence of surgical repair, are often noted in the RV outflow tract and contribute to reductions in EF and SV (102).

Probably as a result of all of the aforementioned factors, it has become increasingly evident that chronic volume overload may eventually lead to RV systolic dysfunction and increased morbidity and mortality, particularly in the presence of superimposed pressure overload and/or marked RV enlargement, which argues for corrective interventions before significant RV dilatation ensues

FIGURE 8 Probability of RVRR as a Function of Treatment-Related Decrease in PVR in Pulmonary Arterial Hypertension

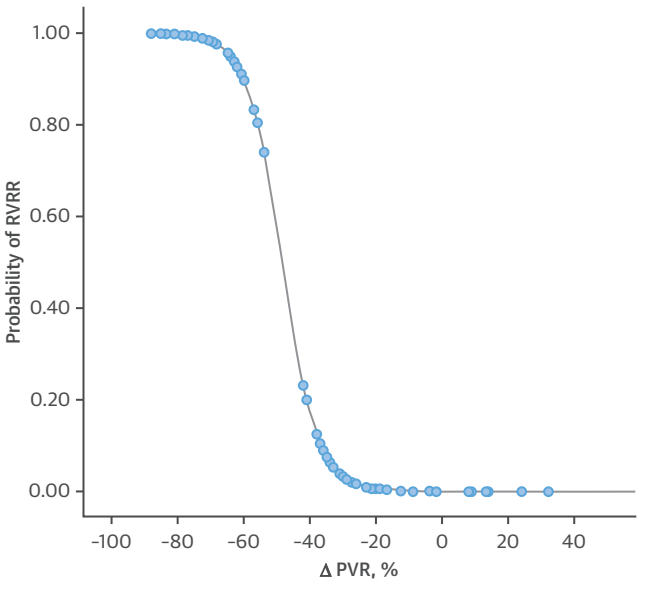

Because of the sigmoid shape of the curve, small additional decreases in PVR from −40% to −50% may result in considerable RV improvement. Data from Badagliacca et al. (89) and van de Veerdonk et al. (90). PVR = pulmonary vascular resistance; RVRR = right ventricular reverse remodeling.

(4). In the case of pulmonary regurgitation in Fallot, studies have consistently identified thresholds of RV EDV and ESV in the vicinity of 160 and 80 ml/m^2, respectively, above which RV functional recovery is less likely (103). Interestingly, a similar threshold of EDV <164 ml/m^2 has been suggested for timing of tricuspid regurgitation repair (104).

THE CARDIOMYOPATHIC RV

Myocardial insults of various etiologies may involve the RV and lead to structural and functional abnormalities. The adaptive response of the RV in this context differs not only according to the underlying pathological process, but importantly, also according to any associated volume and/or pressure overload. Similarly, a component of myopathic RV involvement may explain worse adaptation to PH in certain conditions such as scleroderma (74).

ISCHEMIC HEART DISEASE. Postmortem, RV involvement can be detected in up to 50% of acute myocardial infarctions (105), suggesting that RV infarct is often underdiagnosed. Contemporary series of consecutive patients with reperfused acute infarction have identified RV late gadolinium enhancement, consistent with necrosis, in 10% to 30% of patients, and edema in up to 50% (106,107). The presence of microvascular obstruction, however, is extremely rare (107). RV injury is more common and extensive in inferior infarcts but is also present in a substantial proportion of anterior infarcts (106). After the acute phase, RV function tends to recover, suggesting that, due to the relatively resistance to ischemia described in the previous text, chronic RV infarcts are infrequent. However, healed infarcts are not rare in autopsy series (105), and are identified in vivo in 5% to 13% of patients with magnetic resonance (106,108,109) (**Figure 9A**). The prevalence of chronic RV dysfunction has ranged between 17% and 60% in different reports depending on the definition employed, and it is uncertain if chronic scars carry prognostic significance beyond that of decreased RV EF (108,109). Because of the relatively low prevalence of chronic scars, it is likely that post-infarction RV dysfunction is multifactorial in etiology, including LV-RV interactions, increased afterload, ischemia, and mitral regurgitation (109).

ARRHYTHMOGENIC CARDIOMYOPATHY. It is traditionally considered that fibrofatty replacement in arrhythmogenic cardiomyopathy (**Central Illustration**) predominantly involve the so-called "triangle of dysplasia" of the RV free wall (**Figure 9B**), which comprises the infundibulum, subtricuspid region, and apex (110). However, imaging and electroanatomical mapping in proven mutation carriers have recently shown preferential involvement of the RV basal inferior and anterior segments in early disease (as well as the LV basal inferolateral segment; termed "new triangle of dysplasia"), with RV apical involvement only in advanced stages (111). It is widely accepted that electrical abnormalities precede structural derangement, resulting in 3 disease stages: a subclinical or concealed phase (where no abnormalities are identifiable), an electrical phase, and a final structural phase with RV regional or global dilatation and systolic dysfunction (112). Nevertheless, myocardial deformation imaging has demonstrated abnormalities predominantly involving the subtricuspid region in asymptomatic carriers, including those in the concealed stage, and which have been linked to disease progression (113). To evaluate whether these deformation abnormalities are secondary to electrical disease, 84 mutation carriers (21 in the subclinical stage) were studied with speckle tracking echocardiography. Three patterns of subtricuspid RV longitudinal deformation were identified (**Figure 10**). Abnormal patterns were noted in approximately one-half of carriers in the concealed stage. Interestingly, computer simulations reproduced the abnormal deformation patterns not by changing electrical properties of the system, but only when altered mechanical myocardial characteristics (reduced contractility and increased stiffness) were simulated (**Figure 10**). This suggests that abnormal myocardial deformation is related to subclinical structural disease and challenges the notion that electrical disease necessarily precedes structural abnormalities (114). Spatial heterogeneity in myocardial deformation has additionally been linked to increased arrhythmogenicity (115).

OTHER NONISCHEMIC CARDIOMYOPATHIES. In nonischemic dilated cardiomyopathy, RV dysfunction (defined as EF ≤45%) is present in 35% to 40% of the patients and is also likely multifactorial in origin (116,117). However, RV scar is typically absent (116). In hypertrophic cardiomyopathy, RV hypertrophy is identified with magnetic resonance in approximately one-third of patients and preliminary data suggests that its presence may carry negative prognostic implications (118). RV myocardial disarray predominantly affects the circumferential (superficial) layer, whereas hypertrophy involves mainly the longitudinal aggregates (119). Even when standard indexes of systolic function are normal, RV free wall deformation, diastolic function, and contractile reserve in response to exercise are reduced (120).

FIGURE 9 Magnetic Resonance Images of Different Cardiomyopathies

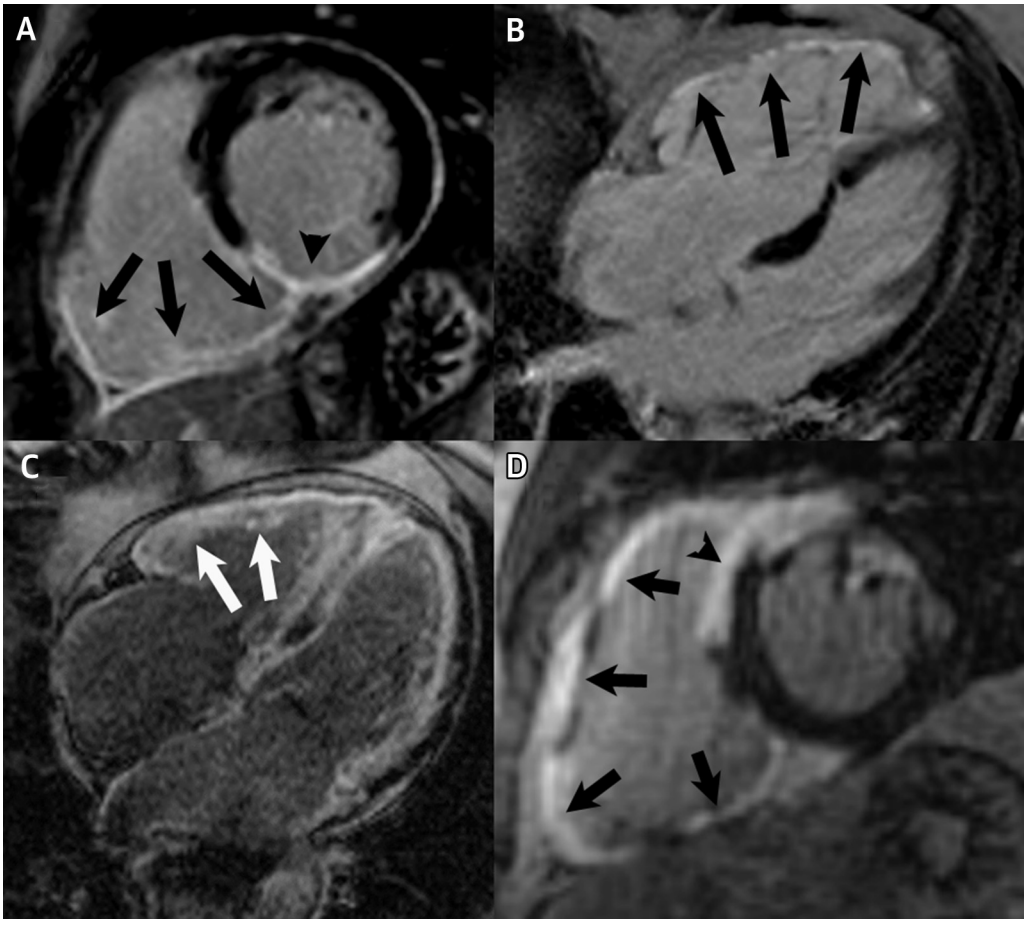

(A) Inferior myocardial infarction **(arrowhead)** with involvement of the right ventricular (RV) inferior wall as demonstrated by late gadolinium enhancement **(arrows)**. **(B)** RV free wall fibrosis **(arrows)** in a patient with arrhythmogenic cardiomyopathy. **(C)** RV enhancement **(white arrows)** secondary to amyloid infiltration. **(D)** Cardiac sarcoidosis with extensive late gadolinium enhancement in the septum **(arrowhead)** and RV free wall **(arrows)**.

In patients with cardiac amyloid, abnormalities in both RV systolic and diastolic function are likely related to RV amyloid deposition, increased load, and, probably most importantly, severity of LV involvement (121). The prevalence of RV infiltration in cardiac amyloidosis is not known, although it is probably common (**Figure 9C**). In a series of 82 patients with an echocardiographic diagnosis of cardiac amyloid, increased RV wall thickness and late enhancement were present in 62% and 61%, respectively (121). Based on limited autopsy data, and opposed to LV amyloid, there is no clear basal-to-apical gradient or preferential subendocardial/trabecular deposition (121,122). In addition, extent of RV infiltration seems to be higher with light-chain than transthyretin amyloid (122).

The frequency of RV involvement in acute myocarditis is not well known, particularly since endomyocardial biopsies are typically obtained from the interventricular septum. In a recent series of 151 consecutive hemodynamically stable patients with acute myocarditis, RV free wall involvement was demonstrated in 18% by the presence of edema and/or late enhancement. RV myocarditis was associated with increased RV volumes and mass, reduced systolic function, and impaired 4-year outcomes (123). In sarcoidosis, late enhancement involving the RV free wall or right aspect of the interventricular septum (**Figure 9D**) can be noted in 15% to 20% of patients with proven extracardiac disease and is associated with RV status as well as PH (124). RV involvement appears to identify a group who are at an

FIGURE 10 **Patterns of Subtricuspid RV Longitudinal Deformation in Carriers of Arrhythmogenic Cardiomyopathy Mutations**

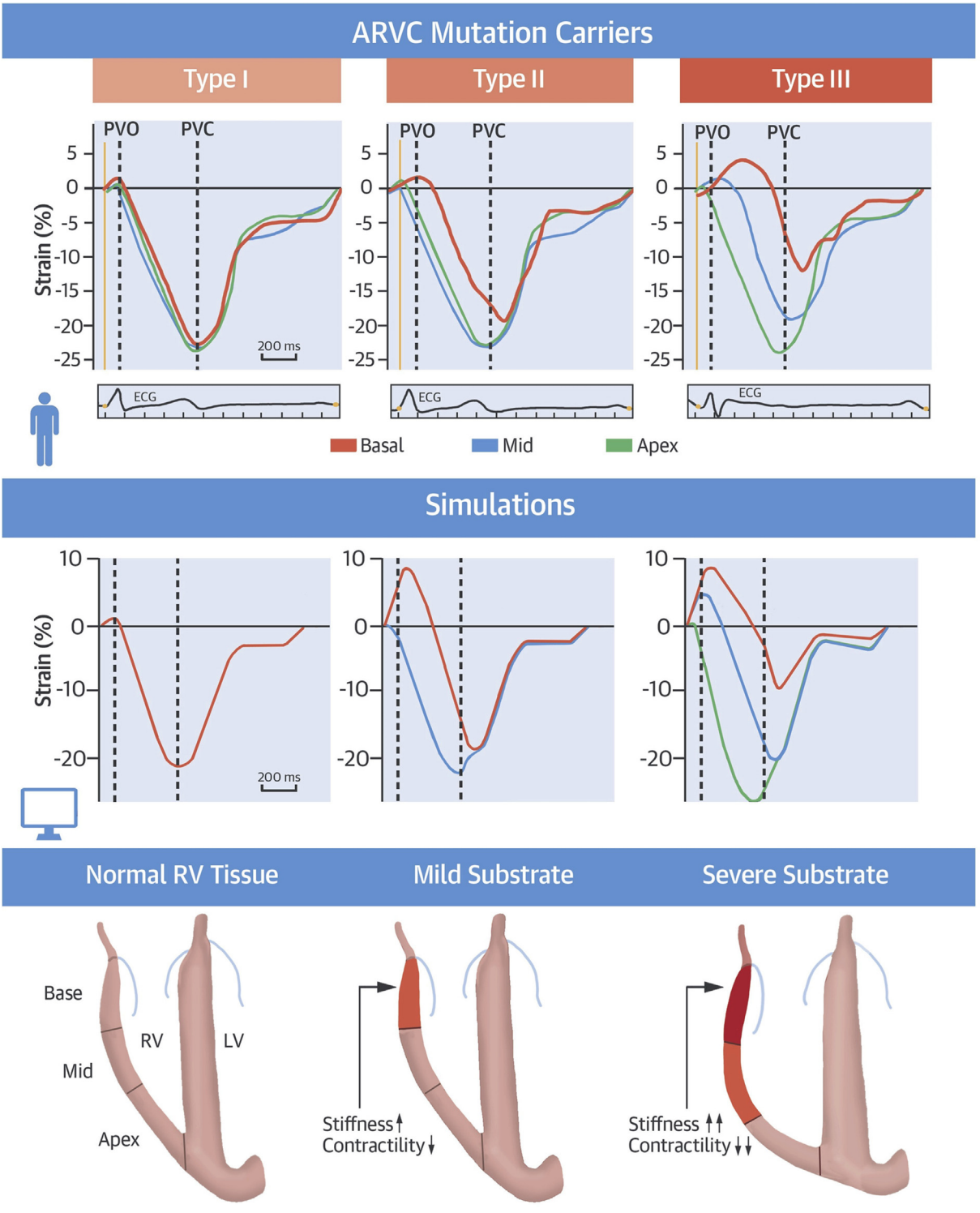

Type I, normal; type II: delayed onset of shortening with reduced peak systolic strain and mild post-systolic shortening; and type III: severely reduced peak systolic strain and post-systolic stretching. Computer simulations reproduced deformation patterns by changing myocardial mechanical properties. Reproduced with permission from Mast et al. (114). ARVC = arrhythmogenic right ventricular cardiomyopathy; ECG = echocardiogram; other abbreviations as in Figures 1 and 2.

especially high risk of ventricular tachyarrhythmia and death (124,125).

CONCLUSIONS

The RV is anatomically and functionally different from the LV, and therefore, our knowledge of LV physiopathology cannot be directly extrapolated to the right heart. The RV plays an essential role in determining symptomatic status and prognosis in nearly all cardiovascular disorders studied to date. Its response to disease is a consequence of various combinations of pressure and/or volume overload as well as intrinsic myocardial deficits, where the predominant abnormality may determine clinical presentation and course. Improving knowledge gaps, recently reviewed elsewhere (23), in our understanding of RV adaption to different conditions is crucial for the development of RV-specific therapies that may ultimately result in improved outcomes.

ACKNOWLEDGMENTS The authors are indebted to Drs. Rebecca Vanderpool and Roberto Badagliacca for their generous assistance with some of the figures in this paper.

ADDRESS FOR CORRESPONDENCE: Dr. Javier Sanz, Mount Sinai Hospital, One Gustave L. Levy Place, Box 1030, New York, New York 10029. E-mail: Javier.Sanz@mountsinai.org. Twitter: @MountSinaiNYC.

REFERENCES

1. Starr I, Jeffers WA, Meade RH. The absence of conspicuous increments of venous pressure after severe damage to the right ventricle of the dog, with a discussion of the relation between clinical congestive failure and heart disease. Am Heart J 1943;26:291–301.

2. Kagan A. Dynamic responses of the right ventricle following extensive damage by cauterization. Circulation 1952;5:816–23.

3. Fontan F, Baudet E. Surgical repair of tricuspid atresia. Thorax 1971;26:240–8.

4. Konstam MA, Kiernan MS, Bernstein D, et al. Evaluation and management of right-sided heart failure: a scientific statement from the American Heart Association. Circulation 2018;137:e578–622.

5. Dell'Italia LJ. The right ventricle: anatomy, physiology, and clinical importance. Curr Probl Cardiol 1991;16:653–720.

6. Kawel-Boehm N, Maceira A, Valsangiacomo-Buechel ER, et al. Normal values for cardiovascular magnetic resonance in adults and children. J Cardiovasc Magn Reson 2015;17:29.

7. Haddad F, Hunt SA, Rosenthal DN, Murphy DJ. Right ventricular function in cardiovascular disease, part I: anatomy, physiology, aging, and functional assessment of the right ventricle. Circulation 2008;117:1436–48.

8. Geva T, Powell AJ, Crawford EC, Chung T, Colan SD. Evaluation of regional differences in right ventricular systolic function by acoustic quantification echocardiography and cine magnetic resonance imaging. Circulation 1998;98:339–45.

9. Alva C, Ho SY, Lincoln CR, Rigby ML, Wright A, Anderson RH. The nature of the obstructive muscular bundles in double-chambered right ventricle. J Thorac Cardiovasc Surg 1999;117:1180–9.

10. Loukas M, Klaassen Z, Tubbs RS, et al. Anatomical observations of the moderator band. Clin Anat 2010;23:443–50.

11. Naeije R, Badagliacca R. The overloaded right heart and ventricular interdependence. Cardiovasc Res 2017;113:1474–85.

12. Kelly RG, Buckingham ME, Moorman AF. Heart fields and cardiac morphogenesis. Cold Spring Harb Perspect Med 2014;4.

13. Kiserud T, Acharya G. The fetal circulation. Prenat Diagn 2004;24:1049–59.

14. Ashley LM. A determination of the diameters of ventricular myocardial fibers in man and other mammals. Am J Anat 1945;77:325–63.

15. Weber KT. Cardiac interstitium in health and disease: the fibrillar collagen network. J Am Coll Cardiol 1989;13:1637–52.

16. Drake JI, Bogaard HJ, Mizuno S, et al. Molecular signature of a right heart failure program in chronic severe pulmonary hypertension. Am J Respir Cell Mol Biol 2011;45:1239–47.

17. Phillips D, Aponte AM, Covian R, Neufeld E, Yu ZX, Balaban RS. Homogenous protein programming in the mammalian left and right ventricle free walls. Physiol Genomics 2011;43:1198–206.

18. Feridooni HA, Dibb KM, Howlett SE. How cardiomyocyte excitation, calcium release and contraction become altered with age. J Mol Cell Cardiol 2015;83:62–72.

19. Kawut SM, Lima JA, Barr RG, et al. Sex and race differences in right ventricular structure and function: the multi-ethnic study of atherosclerosis-right ventricle study. Circulation 2011;123:2542–51.

20. Chia EM, Hsieh CH, Boyd A, et al. Effects of age and gender on right ventricular systolic and diastolic function using two-dimensional speckle-tracking strain. J Am Soc Echocardiogr 2014;27:1079–10786.e1.

21. Ventetuolo CE, Ouyang P, Bluemke DA, et al. Sex hormones are associated with right ventricular structure and function: the MESA-right ventricle study. Am J Respir Crit Care Med 2011;183:659–67.

22. Liu A, Schreier D, Tian L, et al. Direct and indirect protection of right ventricular function by estrogen in an experimental model of pulmonary arterial hypertension. Am J Physiol Heart Circ Physiol 2014;307:H273–83.

23. Lahm T, Douglas IS, Archer SL, et al. Assessment of right ventricular function in the research setting: knowledge gaps and pathways forward. An official American Thoracic Society Research Statement. Am J Respir Crit Care Med 2018;198:e15–43.

24. Ryan JJ, Archer SL. The right ventricle in pulmonary arterial hypertension: disorders of metabolism, angiogenesis and adrenergic signaling in right ventricular failure. Circ Res 2014;115:176–88.

25. Waskova-Arnostova P, Elsnicova B, Kasparova D, et al. Right-to-left ventricular differences in the expression of mitochondrial hexokinase and phosphorylation of Akt. Cell Physiol Biochem 2013;31:66–79.

26. Zong P, Tune JD, Downey HF. Mechanisms of oxygen demand/supply balance in the right ventricle. Exp Biol Med 2005;230:507–19.

27. Calcutteea A, Chung R, Lindqvist P, Hodson M, Henein MY. Differential right ventricular regional function and the effect of pulmonary hypertension: three-dimensional echo study. Heart 2011;97:1004–11.

28. Sengupta PP, Narula J. RV form and function: a piston pump, vortex impeller, or hydraulic ram? J Am Coll Cardiol Img 2013;6:636–9.

29. Fernandez-Friera L, Garcia-Alvarez A, Guzman G, et al. Apical right ventricular dysfunction in patients with pulmonary hypertension demonstrated with magnetic resonance. Heart 2011;97:1250–6.

30. Vitarelli A, Mangieri E, Terzano C, et al. Three-dimensional echocardiography and 2D-3D speckle-tracking imaging in chronic pulmonary hypertension: diagnostic accuracy in detecting hemodynamic signs of right ventricular (RV) failure. J Am Heart Assoc 2015;4:e001584.

31. Fredriksson AG, Zajac J, Eriksson J, et al. 4-D blood flow in the human right ventricle. Am J Physiol Heart Circ Physiol 2011;301:H2344–50.

32. Brown SB, Raina A, Katz D, Szerlip M, Wiegers SE, Forfia PR. Longitudinal shortening accounts for the majority of right ventricular contraction and improves after pulmonary vasodilator therapy in normal subjects and patients with pulmonary arterial hypertension. Chest 2011;140:27–33.

33. Li Y, Xie M, Wang X, Lu Q, Fu M. Right ventricular regional and global systolic function is diminished in patients with pulmonary arterial hypertension: a 2-dimensional ultrasound speckle tracking echocardiography study. Int J Cardiovasc Imaging 2013;29:545–51.

34. Lopez-Candales A, Rajagopalan N, Gulyasy B, Edelman K, Bazaz R. Differential strain and velocity generation along the right ventricular free wall in pulmonary hypertension. Can J Cardiol 2009;25:e73–7.

35. Kind T, Mauritz GJ, Marcus JT, van de Veerdonk M, Westerhof N, Vonk-Noordegraaf A. Right ventricular ejection fraction is better reflected by transverse rather than longitudinal wall motion in pulmonary hypertension. J Cardiovasc Magn Reson 2010;12:35.

36. van Wolferen SA, Marcus JT, Westerhof N, et al. Right coronary artery flow impairment in patients with pulmonary hypertension. Eur Heart J 2008;29:120–7.

37. Paridon SM, Mitchell PD, Colan SD, et al. A cross-sectional study of exercise performance during the first 2 decades of life after the Fontan operation. J Am Coll Cardiol 2008;52:99–107.

38. Naeije R, Brimioulle S, Dewachter L. Biomechanics of the right ventricle in health and disease (2013 Grover Conference series). Pulm Circ 2014;4:395–406.

39. Vonk Noordegraaf A, Westerhof BE, Westerhof N. The relationship between the right ventricle and its load in pulmonary hypertension. J Am Coll Cardiol 2017;69:236–43.

40. Rain S, Handoko ML, Trip P, et al. Right ventricular diastolic impairment in patients with pulmonary arterial hypertension. Circulation 2013;128:2016–25. 1–10.

41. Naeije R, Vanderpool R, Peacock A, Badagliacca R. The right heart-pulmonary circulation unit: physiopathology. Heart Fail Clin 2018;14:237–45.

42. Maughan WL, Shoukas AA, Sagawa K, Weisfeldt ML. Instantaneous pressure-volume relationship of the canine right ventricle. Circ Res 1979;44:309–15.

43. Brimioulle S, Wauthy P, Ewalenko P, et al. Single-beat estimation of right ventricular end-systolic pressure-volume relationship. Am J Physiol Heart Circ Physiol 2003;284:H1625–30.

44. Vanderpool RR, Pinsky MR, Naeije R, et al. RV-pulmonary arterial coupling predicts outcome in patients referred for pulmonary hypertension. Heart 2015;101:37–43.

45. Sanz J, Garcia-Alvarez A, Fernandez-Friera L, et al. Right ventriculo-arterial coupling in pulmonary hypertension: a magnetic resonance study. Heart 2012;98:238–43.

46. Guihaire J, Haddad F, Boulate D, et al. Non-invasive indices of right ventricular function are markers of ventricular-arterial coupling rather than ventricular contractility: insights from a porcine model of chronic pressure overload. Eur Heart J Cardiovasc Imaging 2013;14:1140–9.

47. Tello K, Axmann J, Ghofrani HA, et al. Relevance of the TAPSE/PASP ratio in pulmonary arterial hypertension. Int J Cardiol 2018;266:229–35.

48. Dong Y, Sun J, Yang D, et al. Right ventricular septomarginal trabeculation hypertrophy is associated with disease severity in patients with pulmonary arterial hypertension. Int J Cardiovasc Imaging 2018;34:1439–49.

49. Saremi F, Gera A, Ho SY, Hijazi ZM, Sanchez-Quintana D. CT and MR imaging of the pulmonary valve. Radiographics 2014;34:51–71.

50. Sanchez-Quintana D, Anderson RH, Ho SY. Ventricular myoarchitecture in tetralogy of Fallot. Heart 1996;76:280–6.

51. Tezuka F, Hort W, Lange PE, Nurnberg JH. Muscle fiber orientation in the development and regression of right ventricular hypertrophy in pigs. Acta Pathol Jpn 1990;40:402–7.

52. Nielsen E, Smerup M, Agger P, et al. Normal right ventricular three-dimensional architecture, as assessed with diffusion tensor magnetic resonance imaging, is preserved during experimentally induced right ventricular hypertrophy. Anat Rec (Hoboken) 2009;292:640–51.

53. Park DW, Sebastiani A, Yap CH, Simon MA, Kim K. Quantification of coupled stiffness and fiber orientation remodeling in hypertensive rat right-ventricular myocardium using 3D ultrasound speckle tracking with biaxial testing. PLoS One 2016;11:e0165320.

54. Hopkins WE, Waggoner AD. Severe pulmonary hypertension without right ventricular failure: the unique hearts of patients with Eisenmenger syndrome. Am J Cardiol 2002;89:34–8.

55. Lyon RC, Zanella F, Omens JH, Sheikh F. Mechanotransduction in cardiac hypertrophy and failure. Circ Res 2015;116:1462–76.

56. Sanada S, Hakuno D, Higgins LJ, Schreiter ER, McKenzie AN, Lee RT. IL-33 and ST2 comprise a critical biomechanically induced and cardioprotective signaling system. J Clin Invest 2007;117:1538–49.

57. Bogaard HJ, Abe K, Vonk-Noordegraaf A, Voelkel NF. The right ventricle under pressure; cellular and molecular mechanisms of right heart failure in pulmonary hypertension. Chest 2009;135:794–804.

58. Izumiya Y, Shiojima I, Sato K, Sawyer DB, Colucci WS, Walsh K. Vascular endothelial growth factor blockade promotes the transition from compensatory cardiac hypertrophy to failure in response to pressure overload. Hypertension 2006;47:887–93.

59. Vogel-Claussen J, Skrok J, Shehata ML, et al. Right and left ventricular myocardial perfusion reserves correlate with right ventricular function and pulmonary hemodynamics in patients with pulmonary arterial hypertension. Radiology 2011;258:119–27.

60. Bogaard HJ, Natarajan R, Henderson SC, et al. Chronic pulmonary artery pressure elevation is insufficient to explain right heart failure. Circulation 2009;120:1951–60.

61. Graham BB, Kumar R, Mickael C, et al. Vascular adaptation of the right ventricle in experimental pulmonary hypertension. Am J Respir Cell Mol Biol 2018;59:479–89.

62. Galie N, Saia F, Palazzini M, et al. Left main coronary artery compression in patients with pulmonary arterial hypertension and angina. J Am Coll Cardiol 2017;69:2808–17.

63. Faber MJ, Dalinghaus M, Lankhuizen IM, et al. Proteomic changes in the pressure overloaded right ventricle after 6 weeks in young rats: correlations with the degree of hypertrophy. Proteomics 2005;5:2519–30.

64. Rich S, Pogoriler J, Husain AN, Toth PT, Gomberg-Maitland M, Archer SL. Long-term effects of epoprostenol on the pulmonary vasculature in idiopathic pulmonary arterial hypertension. Chest 2010;138:1234–9.

65. Oikawa M, Kagaya Y, Otani H, et al. Increased [18F]fluorodeoxyglucose accumulation in right ventricular free wall in patients with pulmonary hypertension and the effect of epoprostenol. J Am Coll Cardiol 2005;45:1849–55.

66. Sutendra G, Dromparis P, Paulin R, et al. A metabolic remodeling in right ventricular hypertrophy is associated with decreased angiogenesis and a transition from a compensated to a decompensated state in pulmonary hypertension. J Mol Med (Berl) 2013;91:1315–27.

67. van de Veerdonk MC, Bogaard HJ, Voelkel NF. The right ventricle and pulmonary hypertension. Heart Fail Rev 2016;21:259–71.

68. Rol N, de Raaf MA, Sun X, et al. Nintedanib improves cardiac fibrosis but leaves pulmonary vascular remodeling unaltered in experimental pulmonary hypertension. Cardiovasc Res 2019;115:432–9.

69. Garcia-Alvarez A, Garcia-Lunar I, Pereda D, et al. Association of myocardial T1-mapping CMR with hemodynamics and RV performance in pulmonary hypertension. J Am Coll Cardiol Img 2015;8:76–82.

70. Sanz J, Dellegrottaglie S, Kariisa M, et al. Prevalence and correlates of septal delayed contrast enhancement in patients with pulmonary hypertension. Am J Cardiol 2007;100:731–5.

71. Gomez-Arroyo J, Santos-Martinez LE, Aranda A, et al. Differences in right ventricular remodeling secondary to pressure overload in patients with pulmonary hypertension. Am J Respir Crit Care Med 2014;189:603–6.

72. Vonk-Noordegraaf A, Haddad F, Chin KM, et al. Right heart adaptation to pulmonary arterial hypertension: physiology and pathobiology. J Am Coll Cardiol 2013;62:D22–33.

73. Sun XQ, Abbate A, Bogaard HJ. Role of cardiac inflammation in right ventricular failure. Cardiovasc Res 2017;113:1441–52.

74. Hsu S, Houston BA, Tampakakis E, et al. Right ventricular functional reserve in pulmonary arterial hypertension. Circulation 2016;133:2413–22.

75. Spruijt OA, de Man FS, Groepenhoff H, et al. The effects of exercise on right ventricular contractility and right ventricular-arterial coupling

in pulmonary hypertension. Am J Respir Crit Care Med 2015;191:1050–7.

76. Lamia B, Muir JF, Molano LC, et al. Altered synchrony of right ventricular contraction in borderline pulmonary hypertension. Int J Cardiovasc Imaging 2017;33:1331–9.

77. Walmsley J, van Everdingen W, Cramer MJ, Prinzen FW, Delhaas T, Lumens J. Combining computer modelling and cardiac imaging to understand right ventricular pump function. Cardiovasc Res 2017;113:1486–98.

78. Badagliacca R, Reali M, Poscia R, et al. Right intraventricular dyssynchrony in idiopathic, heritable, and anorexigen-induced pulmonary arterial hypertension: clinical impact and reversibility. J Am Coll Cardiol Img 2015;8:642–52.

79. Marcus JT, Gan CT, Zwanenburg JJ, et al. Interventricular mechanical asynchrony in pulmonary arterial hypertension: left-to-right delay in peak shortening is related to right ventricular overload and left ventricular underfilling. J Am Coll Cardiol 2008;51:750–7.

80. Hayabuchi Y, Ono A, Homma Y, Kagami S. Analysis of right ventricular myocardial stiffness and relaxation components in children and adolescents with pulmonary arterial hypertension. J Am Heart Assoc 2018;7:e008670.

81. Trip P, Rain S, Handoko ML, et al. Clinical relevance of right ventricular diastolic stiffness in pulmonary hypertension. Eur Respir J 2015;45:1603–12.

82. Kuehne T, Yilmaz S, Steendijk P, et al. Magnetic resonance imaging analysis of right ventricular pressure-volume loops: in vivo validation and clinical application in patients with pulmonary hypertension. Circulation 2004;110:2010–6.

83. Axell RG, Messer SJ, White PA, et al. Ventriculo-arterial coupling detects occult RV dysfunction in chronic thromboembolic pulmonary vascular disease. Physiol Rep 2017;5:e13227.

84. Tello K, Richter MJ, Axmann J, et al. More on single-beat estimation of right ventriculo-arterial coupling in pulmonary arterial hypertension. Am J Respir Crit Care Med 2018;198:816–8.

85. Brewis MJ, Bellofiore A, Vanderpool RR, et al. Imaging right ventricular function to predict outcome in pulmonary arterial hypertension. Int J Cardiol 2016;218:206–11.

86. Vanderpool RR, Rischard F, Naeije R, Hunter K, Simon MA. Simple functional imaging of the right ventricle in pulmonary hypertension: can right ventricular ejection fraction be improved? Int J Cardiol 2016;223:93–4.

87. van de Veerdonk MC, Kind T, Marcus JT, et al. Progressive right ventricular dysfunction in patients with pulmonary arterial hypertension responding to therapy. J Am Coll Cardiol 2011;58:2511–9.

88. Vanderpool RR, Desai AA, Knapp SM, et al. How prostacyclin therapy improves right ventricular function in pulmonary arterial hypertension. Eur Respir J 2017;50:1700764.

89. Badagliacca R, Raina A, Ghio S, et al. Influence of various therapeutic strategies on right ventricular morphology, function and hemodynamics in pulmonary arterial hypertension. J Heart Lung Transplant 2018;37:365–75.

90. van de Veerdonk MC, Huis In T Veld AE, Marcus JT, et al. Upfront combination therapy reduces right ventricular volumes in pulmonary arterial hypertension. Eur Respir J 2017;49:1700007.

91. Marino TA, Kent RL, Uboh CE, Fernandez E, Thompson EW, Cooper Gt. Structural analysis of pressure versus volume overload hypertrophy of cat right ventricle. Am J Physiol 1985;249:H371–9.

92. Bartelds B, Borgdorff MA, Smit-van Oosten A, et al. Differential responses of the right ventricle to abnormal loading conditions in mice: pressure vs. volume load. Eur J Heart Fail 2011;13:1275–82.

93. Reddy S, Zhao M, Hu DQ, et al. Physiologic and molecular characterization of a murine model of right ventricular volume overload. Am J Physiol Heart Circ Physiol 2013;304:H1314–27.

94. Otani H, Kagaya Y, Yamane Y, et al. Long-term right ventricular volume overload increases myocardial fluorodeoxyglucose uptake in the interventricular septum in patients with atrial septal defect. Circulation 2000;101:1686–92.

95. Szabo G, Soos P, Bahrle S, et al. Adaptation of the right ventricle to an increased afterload in the chronically volume overloaded heart. Ann Thorac Surg 2006;82:989–95.

96. Kuehne T, Saeed M, Gleason K, et al. Effects of pulmonary insufficiency on biventricular function in the developing heart of growing swine. Circulation 2003;108:2007–13.

97. Redington AN, Rigby ML, Shinebourne EA, Oldershaw PJ. Changes in the pressure-volume relation of the right ventricle when its loading conditions are modified. Br Heart J 1990;63:45–9.

98. Agger P, Ilkjaer C, Laustsen C, et al. Changes in overall ventricular myocardial architecture in the setting of a porcine animal model of right ventricular dilation. J Cardiovasc Magn Reson 2017;19:93.

99. Dragulescu A, Grosse-Wortmann L, Redington A, Friedberg MK, Mertens L. Differential effect of right ventricular dilatation on myocardial deformation in patients with atrial septal defects and patients after tetralogy of Fallot repair. Int J Cardiol 2013;168:803–10.

100. Van De Bruaene A, Buys R, Vanhees L, Delcroix M, Voigt JU, Budts W. Regional right ventricular deformation in patients with open and closed atrial septal defect. Eur J Echocardiogr 2011;12:206–13.

101. Menting ME, van den Bosch AE, McGhie JS, et al. Ventricular myocardial deformation in adults after early surgical repair of atrial septal defect. Eur Heart J Cardiovasc Imaging 2015;16:549–57.

102. Wald RM, Haber I, Wald R, Valente AM, Powell AJ, Geva T. Effects of regional dysfunction and late gadolinium enhancement on global right ventricular function and exercise capacity in patients with repaired tetralogy of Fallot. Circulation 2009;119:1370–7.

103. Heng EL, Gatzoulis MA, Uebing A, et al. Immediate and midterm cardiac remodeling after surgical pulmonary valve replacement in adults with repaired tetralogy of Fallot: a prospective cardiovascular magnetic resonance and clinical study. Circulation 2017;136:1703–13.

104. Kim HK, Kim YJ, Park EA, et al. Assessment of haemodynamic effects of surgical correction for severe functional tricuspid regurgitation: cardiac magnetic resonance imaging study. Eur Heart J 2010;31:1520–8.

105. Andersen HR, Falk E, Nielsen D. Right ventricular infarction: frequency, size and topography in coronary heart disease: a prospective study comprising 107 consecutive autopsies from a coronary care unit. J Am Coll Cardiol 1987;10:1223–32.

106. Masci PG, Francone M, Desmet W, et al. Right ventricular ischemic injury in patients with acute ST-segment elevation myocardial infarction: characterization with cardiovascular magnetic resonance. Circulation 2010;122:1405–12.

107. Grothoff M, Elpert C, Hoffmann J, et al. Right ventricular injury in ST-elevation myocardial infarction: risk stratification by visualization of wall motion, edema, and delayed-enhancement cardiac magnetic resonance. Circ Cardiovasc Imaging 2012;5:60–8.

108. Di Bella G, Siciliano V, Aquaro GD, et al. Right ventricular dysfunction: an independent and incremental predictor of cardiac deaths late after acute myocardial infarction. Int J Cardiovasc Imaging 2015;31:379–87.

109. Sabe MA, Sabe SA, Kusunose K, Flamm SD, Griffin BP, Kwon DH. Predictors and prognostic significance of right ventricular ejection fraction in patients with ischemic cardiomyopathy. Circulation 2016;134:656–65.

110. Gandjbakhch E, Redheuil A, Pousset F, Charron P, Frank R. Clinical diagnosis, imaging, and genetics of arrhythmogenic right ventricular cardiomyopathy/dysplasia: JACC state-of-the-art review. J Am Coll Cardiol 2018;72:784–804.

111. Te Riele AS, James CA, Philips B, et al. Mutation-positive arrhythmogenic right ventricular dysplasia/cardiomyopathy: the triangle of dysplasia displaced. J Cardiovasc Electrophysiol 2013;24:1311–20.

112. te Riele AS, James CA, Rastegar N, et al. Yield of serial evaluation in at-risk family members of patients with ARVD/C. J Am Coll Cardiol 2014;64:293–301.

113. Mast TP, Taha K, Cramer MJ, et al. The prognostic value of right ventricular deformation imaging in early arrhythmogenic right ventricular cardiomyopathy. J Am Coll Cardiol Img 2019;12:446–55.

114. Mast TP, Teske AJ, Walmsley J, et al. Right ventricular imaging and computer simulation for electromechanical substrate characterization in arrhythmogenic right ventricular cardiomyopathy. J Am Coll Cardiol 2016;68:2185–97.

115. Leren IS, Saberniak J, Haland TF, Edvardsen T, Haugaa KH. Combination of ECG and echocardiography for identification of arrhythmic events in early ARVC. J Am Coll Cardiol Img 2017;10:503–13.

116. Gulati A, Ismail TF, Jabbour A, et al. The prevalence and prognostic significance of right ventricular systolic dysfunction in nonischemic

dilated cardiomyopathy. Circulation 2013;128:1623–33.

117. Pueschner A, Chattranukulchai P, Heitner JF, et al. The prevalence, correlates, and impact on cardiac mortality of right ventricular dysfunction in nonischemic cardiomyopathy. J Am Coll Cardiol Img 2017;10:1225–36.

118. Nagata Y, Konno T, Fujino N, et al. Right ventricular hypertrophy is associated with cardiovascular events in hypertrophic cardiomyopathy: evidence from study with magnetic resonance imaging. Can J Cardiol 2015;31:702–8.

119. Kuribayashi T, Roberts WC. Myocardial disarray at junction of ventricular septum and left and right ventricular free walls in hypertrophic cardiomyopathy. Am J Cardiol 1992;70:1333–40.

120. D'Andrea A, Limongelli G, Baldini L, et al. Exercise speckle-tracking strain imaging demonstrates impaired right ventricular contractile reserve in hypertrophic cardiomyopathy. Int J Cardiol 2017;227:209–16.

121. Bodez D, Ternacle J, Guellich A, et al. Prognostic value of right ventricular systolic function in cardiac amyloidosis. Amyloid 2016;23:158–67.

122. Leone O, Longhi S, Quarta CC, et al. New pathological insights into cardiac amyloidosis: implications for non-invasive diagnosis. Amyloid 2012;19:99–105.

123. Aquaro GD, Negri F, De Luca A, et al. Role of right ventricular involvement in acute myocarditis, assessed by cardiac magnetic resonance. Int J Cardiol 2018;271:359–65.

124. Smedema JP, van Geuns RJ, Ector J, Heidbuchel H, Ainslie G, Crijns H. Right ventricular involvement and the extent of left ventricular enhancement with magnetic resonance predict adverse outcome in pulmonary sarcoidosis. ESC Heart Fail 2018;5:157–71.

125. Blankstein R, Osborne M, Naya M, et al. Cardiac positron emission tomography enhances prognostic assessments of patients with suspected cardiac sarcoidosis. J Am Coll Cardiol 2014;63:329–36.

KEY WORDS pulmonary hypertension, right ventricle, right ventricular function